Multi-scale (time and mass) dynamics of space objects
Proceedings IAU Symposium No. 364, 2022
A. Celletti, C. Galeş, C. Beaugé, A. Lemaitre, eds.
doi:10.1017/S1743921321001253

Characterization of the stability for trajectories exterior to Jupiter in the restricted three-body problem via closed-form perturbation theory

Mattia Rossi[1] **and Christos Efthymiopoulos**[2]

[1]Department of Mathematics "Tullio Levi-Civita", University of Padova, Postal Code 35121, Via Trieste 63, Padova, Italy
email: mrossi@math.unipd.it

[2]Department of Mathematics "Tullio Levi-Civita", University of Padova, Postal Code 35121, Via Trieste 63, Padova, Italy
email: cefthym@math.unipd.it

Abstract. We address the question of identifying the long-term (secular) stability regions in the semi-major axis-eccentricity projected phase space of the Sun-Jupiter planar circular restricted three-body problem in the domains i) below the curve of apsis equal to the planet's orbital radius (ensuring protection from collisions) and ii) above that curve. This last domain contains several Jupiter's crossing trajectories. We discuss the structure of the numerical stability map in the (a, e) plane in relation to manifold dynamics. We also present a closed-form perturbation theory for particles with non-crossing highly eccentric trajectories exterior to the planet's trajectory. Starting with a multipole expansion of the barycentric Hamiltonian, our method carries out a sequence of normalizations by Lie series in closed-form and without relegation. We discuss the applicability of the method as a criterion for estimating the boundary of the domain of regular motion.

Keywords. Asteroids, celestial mechanics, n-body simulations

1. Introduction

The secular (long-term) behaviour of the planetary problem, even in the restricted case, is a central question in the framework of the N-body problem. Several heuristic criteria, such as the orbital crossing or the Hill condition (see Ramos *et al.* (2015)) or AMD stability (Laskar & Petit (2017)), have been proposed to discriminate between stable and unstable orbits in phase space. However, there are numerical indications that such methods have some limits as regards their applicability both as a necessary and sufficient condition able to guarantee secular stability.

Here, we first briefly discuss the structure of regular and chaotic regions from a numerical point of view, using short- and long-period Fast Lyapunov Indicator (FLI) stability maps (Lega *et al.* (2016), Guzzo & Lega (2018)) in a very refined grid of initial conditions for the Sun-Jupiter planar circular system (pCR3BP hereafter). As in Todorović *et al.* (2020), we identify arch-like structures and the fractal boundaries discriminating between regular and chaotic orbits. For large values of the semi-major axis and correspondingly increasing eccentricities, a wide set of regular orbits emerges in the FLI diagram. These are clearly protected from collisions and we call them the "lower stability region" (low part of the (a, e) plane).

The main purpose of our semi-analytical work consists of formulating a normalization scheme via closed-form theory capable to deal with considerably high eccentricities and capture topological details of the boundary motion of the lower stability region.

Closed-form perturbation theory provides a framework for series calculations in perturbed Keplerian problems without expansions in powers of the bodies' orbital eccentricities. This is mainly motivated by the necessity to construct secular models for sufficiently eccentric orbits. A main obstruction for the application of closed-form theory in the restricted three-body problem stems from the difficulty to solve the homological equation explicitly when the kernel contains addenda beyond the Keplerian ones. An effective procedure to overcome this issue has been proposed by Deprit *et al.* (2001), called relegation algorithm, which, however, comes with intrinsic poor convergence properties: convergence occurs only in the limit when one of the frequencies is dominant. Such hypothesis cannot be adopted in our case. Hence, in our work we propose a normalization algorithm avoiding relegation supported by numerical verifications, like the accurate reproduction of the orbital elements' variations and detection of mean motion resonances.

The method presented below applies to particles with trajectory completely external to the trajectory of Jupiter. For an analogous method in the case of internal trajectories, see, instead, Cavallari & Efthymiopoulos (this volume of the proceedings).

2. FLI stability map of the Sun-Jupiter pCR3BP

The pCR3BP is defined by the planar motion of a body $\mathcal{P}$ of negligible mass in the gravitation field of two massive bodies $\mathcal{P}_0$ (the primary) and $\mathcal{P}_1$ (the secondary), which perform a circular trajectory around the common barycenter. Let $\vec{R}(t)$ be the barycentric radius vector of the particle and $\vec{r}_1(t)$ the relative radius vector of $\mathcal{P}_1$ with respect to $\mathcal{P}_0$.

The starting Hamiltonian of the model written in barycentric coordinates (i.e. Jacobi variables when $\|\vec{R}\| > \|\vec{r}_1\|$) reads

$$\mathcal{H}(\vec{R}, M_1, \vec{P}, J_1) = \frac{\|\vec{P}\|^2}{2} - \frac{\mathcal{G}m_0}{\|\vec{R} + \mu\vec{r}_1(M_1)\|} - \frac{\mathcal{G}m_1}{\|\vec{R} - (1-\mu)\vec{r}_1(M_1)\|} + n_1 J_1 \,, \qquad (2.1)$$

where $\vec{R} = (X, Y)$, $\vec{P} = (P_X, P_Y) \in T^*(\mathbb{R}^2 \setminus \{-\mu\vec{r}_1, (1-\mu)\vec{r}_1\})$ is the position-momentum couple of $\mathcal{P}$, $\mathcal{G}$ is the gravitational constant, $M_1 = n_1 t$ is the mean anomaly of $\mathcal{P}_1$ (n_1 is the mean motion of the $\mathcal{P}_0, \mathcal{P}_1$ system), J_1 is a dummy action variable canonically conjugate to the angle M_1 and

$$\mu = \frac{m_1}{m_0 + m_1} \in (0, 1/2)$$

is the mass parameter. For a circular trajectory of the primary we have

$$\vec{r}_1(M_1) = \|\vec{r}_1\| \, (\cos M_1, \sin M_1) \ . \qquad (2.2)$$

Figure 1 shows the short-term and long-term FLI stability maps in the semi-major axis-eccentricity (a, e) plane when $\mathcal{P}_0$ is the Sun and $\mathcal{P}_1$ is Jupiter ($\mu = 9.5364 \cdot 10^{-4}$) for particle trajectories computed numerically in the above model. The initial conditions are such that the particle starts orbiting from its pericenter positioned on the X axis.
The top diagram shows how regions of regular orbits permeate the whole phase space, even above the line of pericenter crossing. It is worth noticing that the line of pericenter overestimates the boundary of the lower stability region. This boundary has a fractal shape whose form becomes clearer increasing the integration time, as displayed in bottom panel. Also, mean motion resonances are depicted as spikes penetrating the regular regions of the stability map.

https://doi.org/10.1017/S1743921321001253 Published online by Cambridge University Press

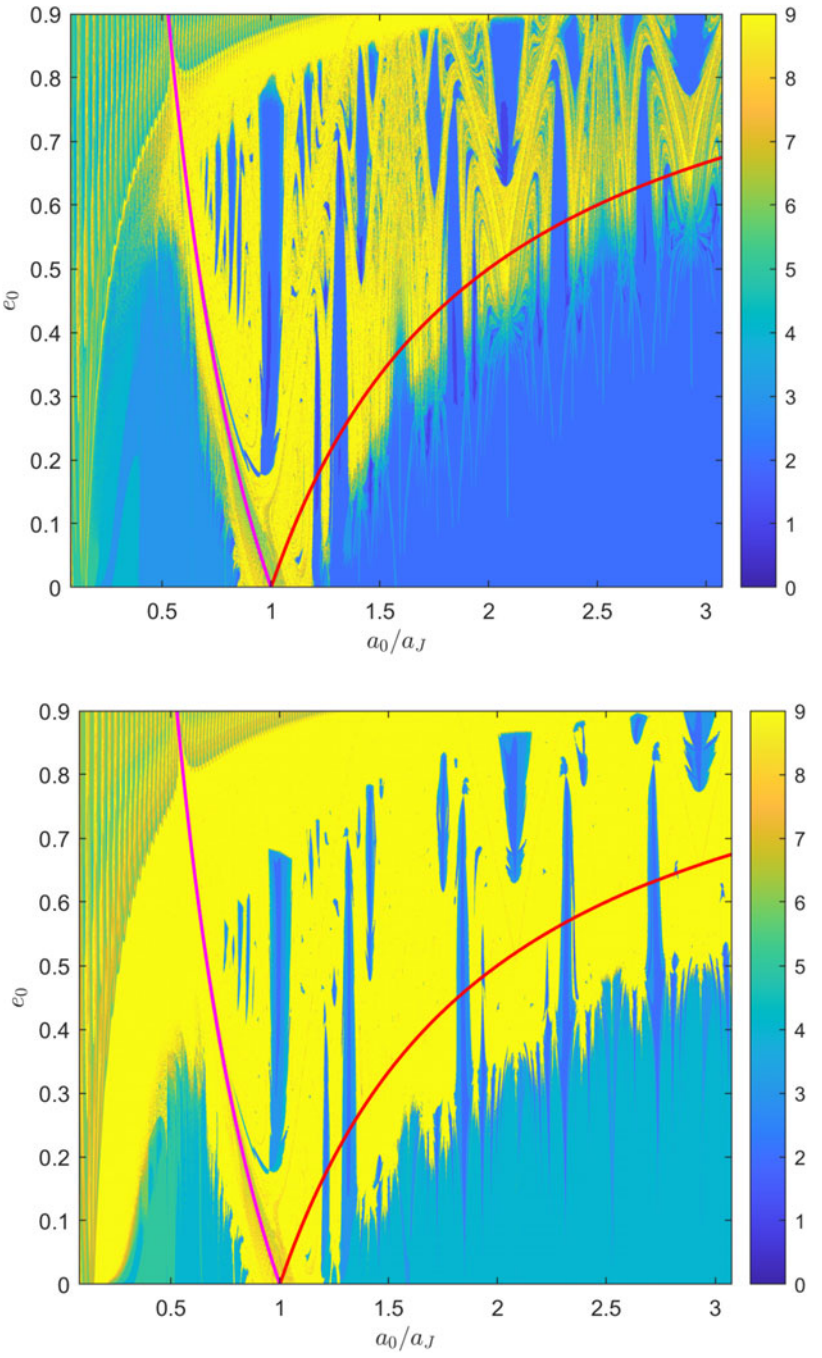

Figure 1. Short-period (top panel) and long-period (bottom panel) FLI maps computed over a grid of 300×900 initial data, where $a_J = \|\vec{r}_1\|$. Integration times are respectively 50 and 1000 Jupiter's orbital periods. The two curves represent the lines of constant apocenter and pericenter of the particle's trajectory equal to a_J.

https://doi.org/10.1017/S1743921321001253 Published online by Cambridge University Press

We also observe in the same plot intricate structures created by the manifolds of the unstable orbits of various mean motion resonances (the "arches of chaos", see Todorović *et al.* (2020)).

3. Closed-form method for trajectories exterior to the trajectory of Jupiter

Assuming $\|\vec{r}_1\|/\|\vec{R}\| \ll 1$, we introduce a book-keeping symbol σ, with numerical value equal to 1, that keeps trace of the order of magnitude of the eccentricity e and of the small mass ratio μ at the same time via the powers σ^1, σ^ν. Expanding (2.1) up to $\mathcal{O}(\mu^{k_\mu}, (\|\vec{r}_1\|/\|\vec{R}\|)^{k_{\rm mp}})$, for $k_\mu, k_{\rm mp} \in \mathbb{N}\setminus\{0\}$ with $k_\mu > 1$, we pass to Delaunay elements (ℓ, g, L, G), defined by

$$\begin{aligned} L &= \sqrt{\mathcal{G}m_0 a}\,, & \ell &= M\,, \\ G &= L\sqrt{1-e^2}\,, & g &= \omega\,, \end{aligned} \tag{3.1}$$

where a, M, ω stand for the semi-major axis, the mean anomaly and the argument of pericenter respectively. We then write $L = L_* + \delta L$, $L_* = \sqrt{\mathcal{G}m_0 a_*}$ and $n_* = \sqrt{\mathcal{G}m_0}a_*^{-3/2}$ for constant reference values a_*, e_* dependent on initial conditions.

Given the above definitions, we have the following.

Proposition. *There exists a canonical transformation conjugating* (2.1) *to the secular normal form with respect to the fast angles* f, M_1 *of the system provided by*

$$\mathscr{H} = \mathscr{H}_0 + \mathscr{R}\,, \tag{3.2}$$

with

$$\mathscr{H}_0 = n_*\delta L - \frac{3n_*}{2L_*}\delta L^2 + n_1 J_1 + \sum_{j=\nu}^{\nu k_\mu - 1} c_j(\delta L, e; \mu)\sigma^j + \mathcal{O}(\delta L^3)\,, \tag{3.3}$$

$$\begin{aligned} \mathscr{R} = &\sum_{\substack{s\in\mathbb{Z}^3 \\ s=(s_1,s_2,s_3)}} d_{\nu k_\mu, s}(\delta L, e; \mu)\cos(s_1 f + s_2 g + s_3 M_1)\sigma^{\nu k_\mu} \\ &+ \mathcal{O}\left(\sigma^{\nu k_\mu + 1}; \left(\frac{\|\vec{r}_1\|}{\|\vec{R}\|}\right)^{k_{mp}+1}, \delta L^3\right)\,, \end{aligned} \tag{3.4}$$

where f *denotes the particle's true anomaly and*

$$\nu = \left\lceil \frac{\log_{10}\mu}{\log_{10} e_*} \right\rceil\,, \tag{3.5}$$

for $c_j, d_{\nu k_\mu, s} \in \mathbb{R}$.

The details of the proof of the above proposition will be presented elsewhere (Rossi & Efthymiopoulos, in preparation). Briefly, expanding the Hamiltonian in power series of the quantity $\delta L = L - L_*$, we obtain

$$\begin{aligned} \mathcal{H} &= -\frac{\mathcal{G}^2 m_0^2}{2L_*^2}\sum_{l=1}^{\infty} l\left(-\frac{\delta L}{L_*}\right)^{l-1} + n_1 J_1 + \mu\sum_{l=0}^{\infty}\frac{1}{l!}\left.\frac{\partial^l \mathcal{H}_1}{\partial L^l}\right|_{L=L_*}\delta L^l \\ &= n_*\delta L + n_1 J_1 + \mu\left(\mathcal{H}_1|_{\delta L=0,\ \mu=0} + \left.\frac{\partial\mathcal{H}_1}{\partial\delta L}\right|_{\delta L=0,\ \mu=0}\delta L\right) + \mathcal{O}(\mu^2, \delta L^2)\,, \end{aligned} \tag{3.6}$$

https://doi.org/10.1017/S1743921321001253 Published online by Cambridge University Press

where we drop the constant $-\mathcal{G}^2 m_0^2/(2L_*^2)$, and $n_* = \mathcal{G}^2 m_0^2/L_*^3$, with the function $\mathcal{H}_1$ given by

$$\mathcal{H}_1 = -\frac{\mathcal{G}m_0}{\|\vec{R}\|} + \mathcal{O}\left(\left(\frac{\|\vec{r}_1\|}{\|\vec{R}\|}\right)^2, \mu^2\right) . \tag{3.7}$$

Let us rewrite (3.6) in Fourier expansion taking advantage of the periodicity of the angles and making the book-keeping symbol explicit:

$$\mathcal{H} = n_* \delta L + n_1 J_1 + \sum_{s\in\mathbb{Z}^3} q_s(\delta L, e; \mu)\cos(s_1 f + s_2 g + s_3 M_1)\sigma_s \tag{3.8}$$

where $\sigma_s \in \{\sigma^\nu, \sigma^{\nu+1}, \ldots\}$ and, by D'Alembert rules, only cosines and real coefficients q_s appear.

Setting $\mathscr{Z}_0 = n_*\delta L + n_1 J_1$ and $\mathscr{R}_\nu^{(0)} = \mathcal{O}(\sigma^\nu)$ the remaining summation in (3.8), we define the Lie series operator by

$$\exp(\mathcal{L}_\chi) = \sum_{n\geq 0} \frac{1}{n!}\mathcal{L}_\chi^n = \mathbb{I} + \mathcal{L}_\chi + \frac{1}{2}\mathcal{L}_\chi \circ \mathcal{L}_\chi + \ldots , \tag{3.9}$$

where $\mathcal{L}_\chi \cdot = \{\cdot, \chi\}$ is the Poisson bracket operator.

Applying (3.9) to (3.8) we get the first transformed Hamiltonian

$$\mathscr{H}^{(1)} = \mathscr{Z}_0 + \mathscr{R}_\nu^{(0)} + \{\mathscr{Z}_0, \chi_\nu^{(1)}\} + \{\mathscr{R}_\nu^{(0)}, \chi_\nu^{(1)}\} + \frac{1}{2}\{\{\mathcal{H}, \chi_\nu^{(1)}\}, \chi_\nu^{(1)}\} + \ldots \tag{3.10}$$

with respect to the generating function $\chi_\nu^{(1)}$, found out as solution of the homological equation

$$\{\mathscr{Z}_0, \chi_\nu^{(1)}\} + \mathscr{R}_\nu^{(0)} = \mathcal{O}(\sigma^{\nu+1}) \tag{3.11}$$

which cancels out σ^ν-terms.

By means of an appropriate rearrangement of the Poisson structure using the chain rule, one can show that

$$\chi_\nu^{(1)} = \sum_{\substack{s\in\mathbb{Z}^3 \\ (s_1,s_3)\neq(0,0)}} \frac{q_{s_\nu}}{s_1 n_* + s_3 n_1}\sin(s_1 f + s_2 g + s_3 M_1)\sigma^\nu , \tag{3.12}$$

with coefficients $q_{s_\nu} = \mathcal{O}(\sigma^\nu)$.

The procedure can be repeated at successive normalization steps.

4. Numerical tests

We consider the example reported in Figure 2. The left panel shows in logarithmic scale the quantity:

$$\mathscr{E}^{(j)} = \sum_{l=\nu+j}^{\nu k_\mu} \sum_{s\in\mathbb{Z}^3} |d_{l,s}^{(j)}| \geq \|\mathscr{R}_{\nu+j}^{(j)}\|_\infty , \quad j = 1, \ldots, \nu(k_\mu - 1) , \tag{4.1}$$

where $\|\cdot\|_\infty$ is the sup norm, j is the number of normalization steps and $\mathscr{R}_{\nu+j}^{(j)} = \mathcal{O}(\sigma^{\nu+j})$ is the normal form remainder of the j-th order.

The plot gives an estimate of the error of the semi-analytical method at the j-th step. The right panel shows a remarkably good agreement of the evolution of the semi-major axis $a(t)$ between a direct integration of the Cartesian equations of motion and a semi-analytic integration using the normal form part of (3.3).

Figure 3, finally, shows in shade scale the size of the remainder as a function of (a, e). We observe that the semi-analytical method allows to define with good precision the

https://doi.org/10.1017/S1743921321001253 Published online by Cambridge University Press

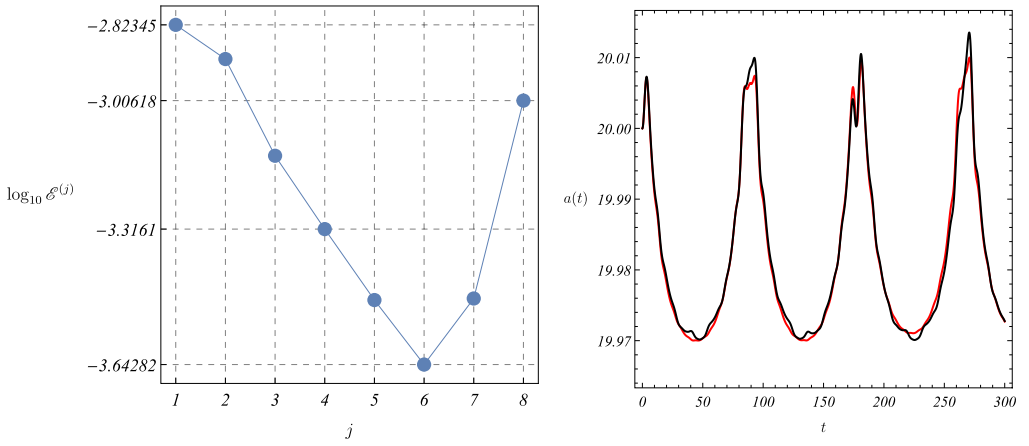

Figure 2. (Left) Evolution of the size of the remainder of the normal form construction of Section 3 as a function of the normalization order j, in an example with $a_* = 20$, $e_* = 0.4$ ($\nu = 8$), $k_\mu = 2$, $k_{\rm mp} = 3$ and order of δL expansion equal to 1. (Right) Comparison of the semi-analytic (dark curve) with the numerical propagation (light curve) of a trajectory.

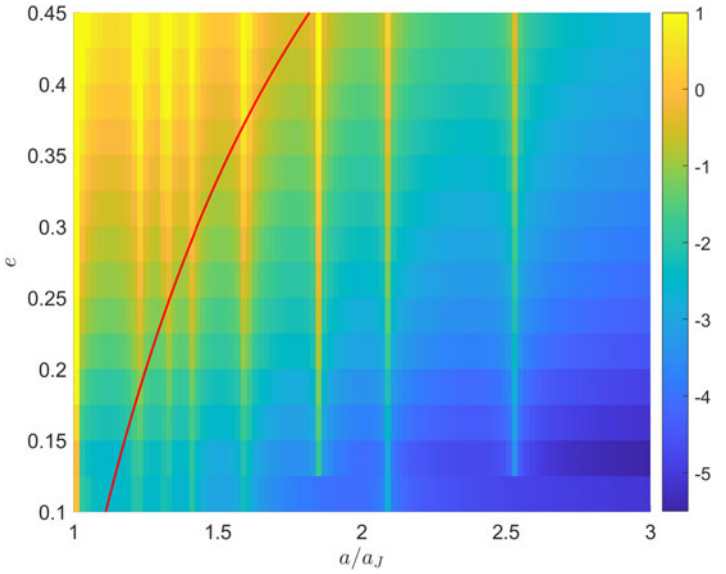

Figure 3. Computation of $\log_{10}(\mathscr{E}^{(\nu(k_\mu-1))})$ over a 100×15 (a, e) grid. For every $e = e_*$ a different normalization is derived and then evaluated for each $a = a_*$. The traced curve is again the constant pericenter line.

lower stability region in Figure 1: the error increases for trajectories close to Jupiter's orbit. The vertical strips correspond to mean motion resonances, as illustrated also in the FLI maps.

Acknowledgements

C.E. was partially supported by the MIUR-PRIN 20178CJA2B New Frontiers of Celestial Mechanics: Theory and Applications.

https://doi.org/10.1017/S1743921321001253 Published online by Cambridge University Press

References

Deprit, André, Palacián, Jesúus & Deprit, Etienne 2001, *Cel. Mech. and Dyn. Astron.*, 79, 157–182

Guzzo, Massimiliano & Lega, Elena 2018, *Physica D: Nonlin. Phen.*, 373, 38–58

Lara, Martin, San-Juan, Juan F. & López-Ochoa, Luis M. 2013, *Mathem. Problems in Engin.*

Laskar, Jacques & Petit, AC 2017, *A&A*, 605, A72

Lega, Elena, Guzzo, Massimiliano & Froeschlé, Claude 2016, *Chaos Detec. and Predict.*, 35–54

Libert, Anne-Sophie & Sansottera, Marco 2013, *Cel. Mech. and Dyn. Astron.*, 117, 149–168

Métris, G & Exertier, Pierre 1995, *A&A*, 294, 278–286

Palacián, Jesús 2002, *Journal of Diff. Equat.*, 180, 471–519

Ramos, Ximena Soledad, Correa-Otto, Jorge Alfredo & Beauge, Cristian 2015, *Cel. Mech. and Dyn. Astron.*, 123, 453–479

Sansottera, Marco & Ceccaroni, Marta 2017, *Cel. Mech. and Dyn. Astron.*, 127, 1–18

Todorović, Nataša, Wu, Di & Rosengren, Aaron J 2020, *Science advances*, 6, eabd1313